Acoustically Coupled Thickness-Mode AlN-on-Si Band-Pass Filters—Part I: Principle and Devices

Wanling Pan, *Member, IEEE*, Vikram A. Thakar, *Member, IEEE*,
Mina Rais-Zadeh, *Senior Member, IEEE*, and Farrokh Ayazi, *Senior Member, IEEE*

***Abstract*—In this, the first of two papers, we present the working principle and the implementation of laterally acoustically coupled thickness-mode thin-film piezoelectric-on-substrate (TPoS) filters. This type of filter offers low insertion loss and small bandwidth in a broad frequency range—from a few hundred megahertz up to a few gigahertz—and occupy a small chip area. In this paper, we discuss several design concerns, including the choice of materials for TPoS filters. We demonstrate a design for an air-suspended AlN-on-Si filter, which offers a low insertion loss of 2.4 dB at 2.877 GHz. The bandwidth of this filter is 12 MHz with a return loss of better than 30 dB. In Part II of this paper, we present a comprehensive analysis of the effect of physical layout parameters on the frequency response of TPoS filters.**

I. Introduction

Micromachined acoustic resonators and filters have been widely investigated for wireless communication applications [1]–[5]. Over the last decade, SAW devices have been successfully implemented in commercial handheld electronics. The working frequency of SAW devices is determined by the lateral pitch of their interdigitated electrodes, which is in turn limited by the lithography resolution. Although higher working frequencies have been achieved, the frequency of commercial SAW filters is typically limited to about 2 GHz [4]. In contrast, acoustic devices working in the thickness vibration mode are not restricted by the lateral resolution and can reliably work at frequencies beyond 2 GHz. Typical thickness-mode acoustic filter architectures include electrically-coupled resonator filters [such as ladder-type film bulk acoustic resonator (FBAR) filters] and acoustically coupled resonator filters [3]. Compared with the ladder-type FBAR filters, which usually need several stages of resonators and have a chip size in the order of 1×1 mm [1], acoustically coupled filters eliminate the large feedthrough capacitance from the input to the output and provide good out-of-band rejection within a compact microstructure. Micromachined thin-film piezoelectric-on-substrate (TPoS) filters based on acoustically coupled resonators have been investigated in previous work [6]–[8]. Fig. 1 schematically shows the cross section of a TPoS filter, in which two or more resonating sections of a low-loss material (i.e., the substrate) are coupled to one another. A thin piezoelectric film laid on the substrate enables electromechanical transduction. The use of a substrate enables lower frequencies to be reached, without having to deposit or grow thick piezoelectric layers, and enhanced power handling. In addition, by adjusting the thickness of the substrate layer (e.g., through oxidation or etching), multiple frequency filters can be implemented on a common substrate while using the same piezoelectric film thickness for all the devices [7], representing a pathway toward filter arrays on-a-chip.

This work presents the design and measured results of low-loss acoustically coupled thickness-mode AlN-on-Si filters for the first time. Earlier work has concentrated on the use of ZnO in TPoS filters and offered very limited design analysis [6]–[8]. Aluminum nitride exhibits a smaller damping factor than ZnO [9] and can improve the insertion loss as well as the out-of-band rejection of TPoS filters. In Part I of the two papers, we explain the working principle of the device on the basis of Lamb wave dispersion. We further report on the fabrication and performance characterization of an AlN-on-Si filter and demonstrate improved performance compared with their ZnO-on-Si counterparts. Specifically, as a proof of concept, a 2.877-GHz AlN-on-Si filter with dimensions as presented in Fig. 1 is demonstrated; it exhibits an insertion loss of 2.4 dB and bandwidth of 12 MHz. To our knowledge, this is among the lowest insertion losses reported for thin-film bulk acoustic filters in the gigahertz regime.

In Part II of this paper [10], we present detailed simulation results to show the relationship between the top electrode geometry and the frequency response of a TPoS filter, such as its bandwidth and insertion loss.

II. Working Principle

A thickness-mode TPoS filter consists of two interdigitated top electrodes (input and output), a solid bottom ground electrode, and a thin layer of a piezoelectric material deposited on a substrate (Fig. 1). In this work, we utilize the thickness-extensional mode of the two electroded

Manuscript received February 9, 2012; accepted June 27, 2012. This work was partially supported by the Defense Advanced Research Projects Agency (DARPA) Analog Spectral Processors (ASP) program and the University of Michigan.

W. Pan was with the Georgia Institute of Technology, Atlanta, GA. He is now with Integrated Device Technology Inc., San Jose, CA.

V. A. Thakar and M. Rais-Zadeh are with the Department of Electrical Engineering and Computer Science, University of Michigan, Ann Arbor, MI (e-mail: thakar@umich.edu).

F. Ayazi is with the School of Electrical and Computer Engineering, Georgia Institute of Technology, Atlanta, GA.

DOI http://dx.doi.org/10.1109/TUFFC.2012.2451

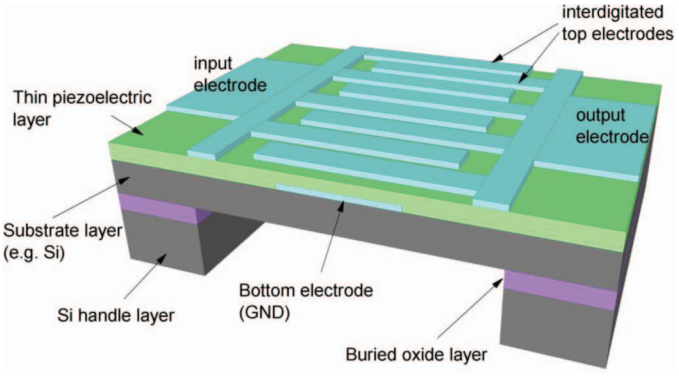

Fig. 1. Schematic view of an acoustically coupled thickness-mode thin-film piezoelectric-on-substrate (TPoS) filter. The resonating sections are the areas defined by the input and output electrode fingers. The substrate layer is part of the resonating stack and is a 5-μm-thick high-resistivity (>1 kΩ·cm) silicon device layer of an SOI wafer. Aluminum nitride 1 μm thick is used as the piezoelectric layer and 100-nm molybdenum is used as the top and bottom electrode material.

regions defined by input and output electrodes. These two regions are coupled via evanescent acoustic waves in the unelectroded region. Such a design takes advantage of the high electromechanical coupling of the piezoelectric layer and the low mechanical damping in the substrate material to achieve low loss. Multiple thickness-extensional modes can be excited; we select the mode order and the corresponding frequency based on the electromechanical coupling factor, which is given by [11]

$$k^2 = \frac{\pi}{2} \cdot \frac{f_s}{f_p} \cdot \tan\left[\frac{\pi}{2} \cdot \frac{(f_p - f_s)}{f_p}\right], \tag{1}$$

where f_s and f_p are the series and parallel thickness-extensional resonance frequencies, respectively. These frequencies can be approximately calculated using the Mason's model [12]. The calculated coupling factors of the first six modes of the electroded stack presented in Fig. 1 are listed in Table I. It is seen that the fourth and the fifth modes have the largest k^2 and are therefore favorable for our filter application. In this work, we choose to focus on the fourth-order mode with a frequency of ~2.9 GHz.

For a given stack, the Lamb wave dispersion curves can be computed using the Thomson–Haskell matrix technique [13]. Fig. 2 shows a part of the dispersion curves around the fourth-order thickness-extensional mode for the TPoS filter having the stack dimensions noted in the caption of Fig. 1. The frequency estimated using Mason's model corresponds to the cut-off point in the dispersion curves where the TE lateral wavenumber is zero. All later-

TABLE I. Electromechanical Coupling Factor of the Thickness-Extensional Modes for the Electroded Stack Presented in Fig. 1.

Mode	1st	2nd	3rd	4th	5th	6th
k^2 (%)	0.12	0.3	0.57	1.28	1.64	0.65
f_s (MHz)	615	1331	2077	2772	3347	3987

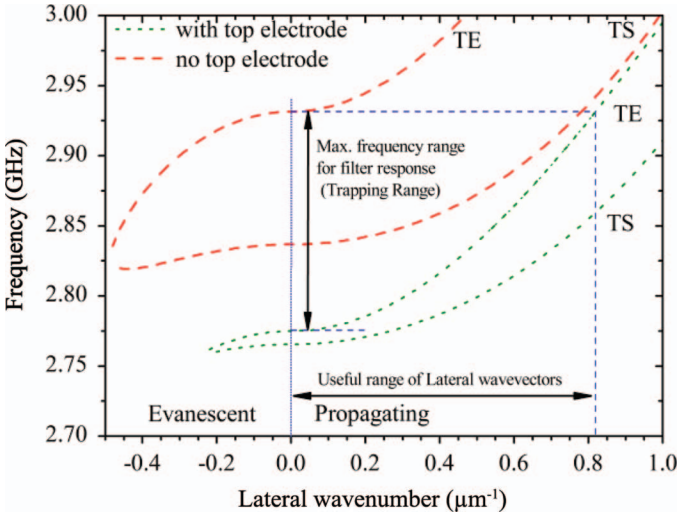

Fig. 2. Dispersion curves of the fourth-order thickness-extensional (TE) mode and the nearest thickness-shear (TS) mode for the stack shown in Fig. 1. The curves are computed using the Thomson–Haskell matrix technique with the thickness, Young's modulus, Poisson's ratio, and mass density of layers as inputs.

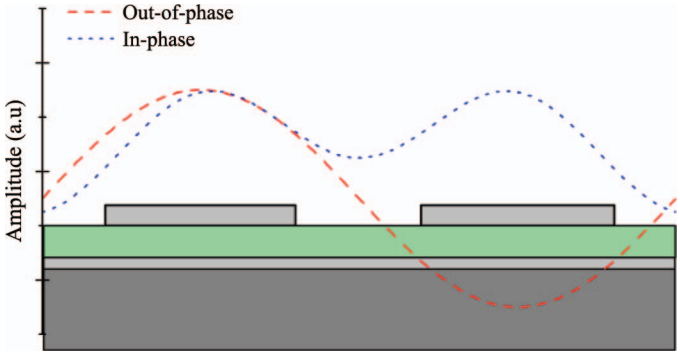

Fig. 3. Lateral waves coupling input and output electrodes with wavelengths corresponding to in-phase and out-of phase modes, superimposed over a two electrode section for clarity.

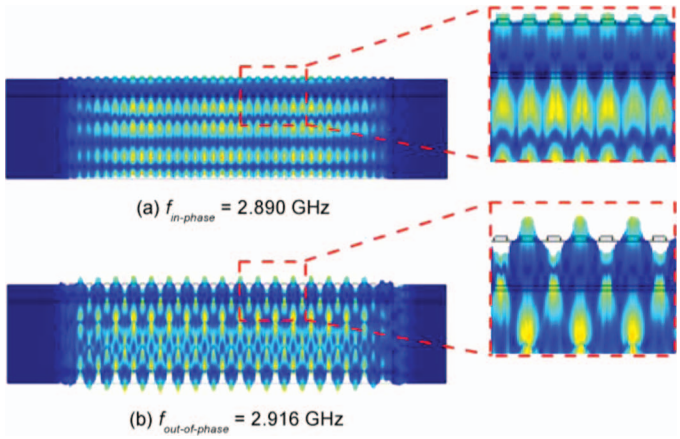

Fig. 4. (a) In-phase and (b) 180° out-of-phase modes of a thickness-mode thin-film piezoelectric-on-substrate (TPoS) filter simulated using Comsol; the modal simulations are performed using the setup presented in Part II of this paper. The color spectrum plots the displacement. The two electroded regions are acoustically coupled, and the coupling between them defines the filter bandwidth. The top electrode consists of 38 fingers with electrode width and spacing of 5 μm each.

al waves emanating from input electrode fingers and supported by the unelectroded region (via evanescent waves) can be coupled to the output electrode [13]. The overall frequency response of the filter can be obtained by charge summation over the electrodes because of the superposition of all supported lateral waves [2], [14]. Thus, the filter frequency response depends on the dispersion relations, and the insertion loss depends on both the electromechanical coupling in each electroded region and the lateral coupling between the two regions. As seen in Fig. 2, for the presented TPoS stack, the frequencies supporting lateral coupling are between 2.77 and 2.93 GHz, corresponding to lateral wavenumbers between 0 and 0.82 μm^{-1}, or lateral wavelengths larger than 7.66 μm in the electroded region. Top electrode geometries allowing constructive interference over this range of wavelengths would provide the maximum bandwidth.

In the passband of the TPoS filter, the two electroded regions vibrate in the thickness extensional mode, either in-phase or 180° out-of-phase (Fig. 3). The two modes are acoustically coupled, resulting in a filter response. The corresponding in-phase and out-of-phase modes for an exemplary TPoS filter are simulated using Comsol, a multiphysics finite element analysis software (Comsol Inc., Burlington, MA), and are shown in Fig. 4. The frequency separation between the two modes, and hence the bandwidth of the filter, is set by the top electrode geometry. In Part II, we present simulation results showing the effect of top electrode layout on the filter frequency response.

III. Electrical Modeling

Fig. 5 shows the equivalent electrical circuit conventionally used to model acoustically coupled filters, in particular for monolithic quartz-based filters [15], [16]. Such a circuit model is also applicable to the filters presented in this work.

To mimic the acoustic coupling, the device is modeled by connecting two resonators with a coupling link. The energy oscillations in the two resonators (R_m, L_m, C_m) can be either in-phase or out-of-phase, representing the simplified working principle of acoustically coupled filters. The quality factor and the frequency of the two resonators are modeled to be identical, and the value of the coupling link determines the frequency separation between in-phase and out-of phase modes, i.e., the bandwidth of the filter.

The capacitive path between the input and output electrodes and through the piezoelectric transduction layer sets the signal floor level in these filters and is modeled in the equivalent circuit via feedthrough elements (R_f and C_f). C_p and R_p are used to account for the static capacitance and the resistive leakage between the top electrodes and the ground metal layer, respectively.

IV. Fabrication Process

Fig. 6 shows the fabrication process flow for thickness-mode TPoS filters. The substrate layer can be chosen from

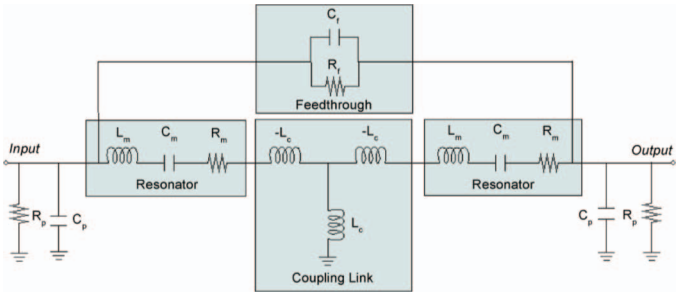

Fig. 5. Equivalent electrical circuit used to model acoustically coupled thin-film piezoelectric-on-substrate (TPoS) filters.

a variety of materials such as silicon (in single-crystal or polycrystalline form), silicon carbide, nanocrystalline diamond [17], silicon dioxide (SiO_2), or even a composite structure, such as one consisting of Si and SiO_2. For filter applications, piezoelectric materials with a large piezoelectric coupling factor and small dielectric constant are preferred, especially at high frequencies. The most commonly used piezoelectric materials that can be micromachined include lead zirconate titanate (PZT), $LiNbO_3$, $LiTaO_3$, ZnO, AlN, and recently GaN [18]. PZT, which has a dielectric constant in the order of a few hundred [19], and $LiNbO_3$ and $LiTaO_3$, which also have considerably larger dielectric constants compared with ZnO or AlN [20], are not the best candidates for high-frequency filter applications. As a consequence, ZnO and AlN (with thickness mode material coupling factor $k_t^2 > 6\%$ and $\varepsilon_r \sim 10$) are better candidates for building TPoS filters. In our earlier work [7], ZnO was used as the piezoelectric material in the filter stack, and insertion loss of less than 6 dB was achieved at frequencies of up to 3 GHz. Sputtered ZnO is

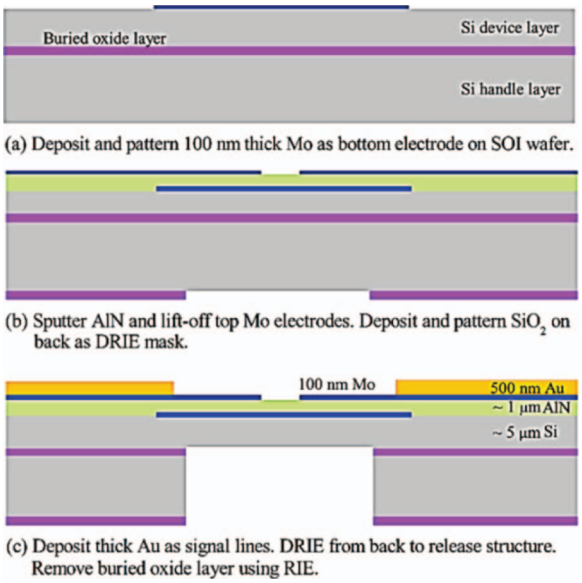

Fig. 6. Fabrication process flow of a thin-film piezoelectric-on-substrate (TPoS) filter [6]. The starting substrate is a high resistivity SOI wafer with Si device layer thickness of 5 ± 0.5 μm. To obtain better device uniformity, commercially available SOI wafers with a tight thickness tolerance (<0.1 μm) or deposited polysilicon can be used.

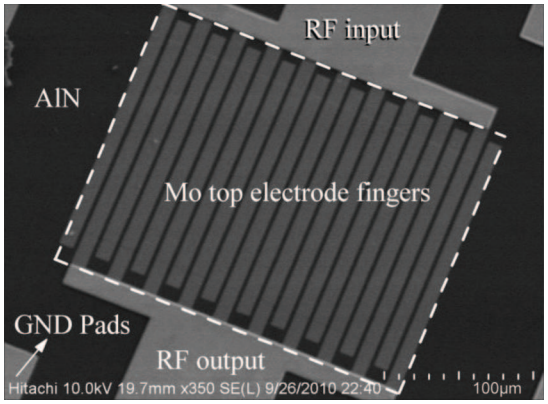

Fig. 7. A scanning electron micrograph of an acoustically coupled thin-film piezoelectric-on-substrate (TPoS) filter. This device has 10 pairs of top electrode fingers with finger length of 150 μm, finger width of 10 μm, and finger spacing of 5 μm.

usually unintentionally doped and therefore has a larger loss tangent (dielectric loss) and smaller resistivity than sputtered AlN [21]. The lower resistivity of ZnO results in more leakage current from the top electrodes to ground (lower R_p in Fig. 5) and larger feedthrough between the input and output ports (larger C_f). Although the leakage current can be reduced by introducing a thin SiO_2 isolation layer between ZnO and the electrodes [6], the large dielectric loss and feedthrough may still degrade the filter performance at high frequencies, causing high insertion loss and elevated out-of-band signal levels. Therefore, AlN, which has lower damping and better isolation, is used in this work to implement filters with better characteristics.

The top input/output electrodes are in interdigitated configuration. Metals with low electrical resistance such as Al and Cu have been used as electrodes in previous work. Compared with Al and Cu, materials with larger specific acoustic impedance, such as W, Mo, or Pt, are usually more favorable for the TPoS structure. The large acoustic impedance of these metals results in high mechanical stress in the piezoelectric layer, and therefore a higher effective electromechanical coupling [22]. Pt and Mo are both well suited for the reactive sputtering of AlN and help achieve a good c–axis orientation for AlN. In this work, we chose Mo over Pt because it is well characterized as a seed layer for AlN deposition. Fig. 7 shows the top view of a fabricated AlN-on-Si TPoS filter.

V. Measurements

On-wafer measurement of filters is carried out at atmospheric pressure using an Agilent N5241A network analyzer with 50 Ω termination (Agilent Technologies Inc., Santa Clara, CA). The RF input power for all of these measurements is −5 dBm unless otherwise stated. Fig. 8(a) shows the measured S-parameters of the filter shown in Fig. 7 having the same stack thicknesses presented in Fig. 1. The top electrode consists of 10 pairs of electrode fingers, each 10 μm wide and separated by an inter-electrode spacing of 5 μm. This filter has an insertion loss of 2.4 dB at 2.877 GHz and a 3-dB bandwidth of 12 MHz. Fig. 8(b) shows the measured phase of S_{21} for the same filter.

Fig. 9 shows the measured filter response superimposed over the dispersion curves for comparison. From the figure, one can see that the composite stack can support traveling waves in the electroded region, which are evanescently coupled in the unelectroded region in a frequency range (shaded region) much larger than the bandwidth of this filter. Therefore, larger bandwidth should be achievable by designing the top electrode geometries (e.g., electrode spacing and electrode finger width). Fig. 10 shows the measured response of another filter consisting of 20 pairs of electrode fingers, each 10 μm wide and separated by 5 μm spacing. The filter exhibits a slightly larger bandwidth with a smaller passband ripple, but has a marginally higher insertion loss.

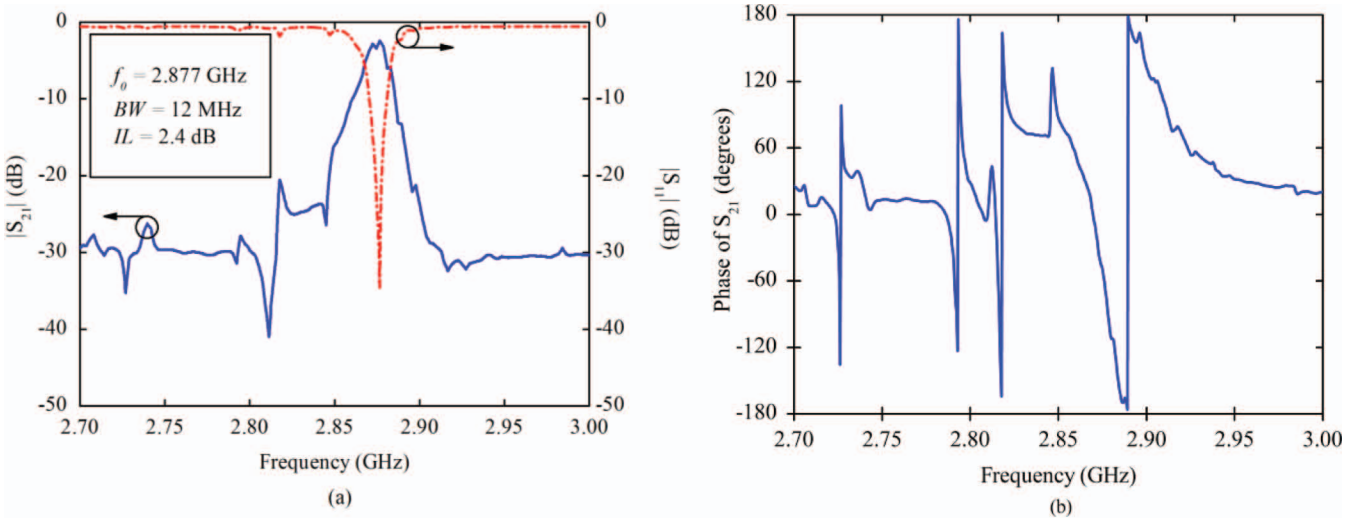

Fig. 8. Measured (a) magnitude and (b) phase of S_{21} for the AlN-on-Si filter shown in Fig. 7. The top electrode consists of 10 pairs of electrode fingers, each 10 μm wide with 5 μm of interelectrode spacing.

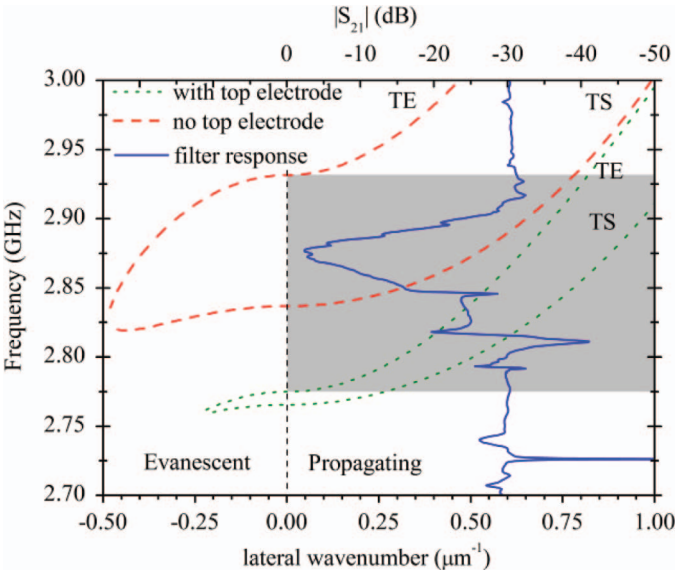

Fig. 9. The dispersion plot for the thin-film piezoelectric-on-substrate (TPoS) filter stack shown in Fig. 1. The measured filter response is superimposed for ease of comparison. From the plot, one can see that lateral waves with wavenumbers between 0.59 and 0.706 μm^{-1} in the electroded region contribute to the measured response.

The frequency response of an AlN-based filter was compared with one using ZnO as the piezoelectric layer, both working in a similar frequency range. Fig. 11 shows the frequency response of a 2.9-GHz ZnO-on-Si filter, the details for which are presented in [7]. It is seen that by replacing ZnO with AlN, not only the loss is improved by almost 3 dB, but the out-of-band signal floor is also improved from −18 dB to −30 dB.

Both AlN-on-Si and ZnO-on-Si filter responses are modeled using the equivalent circuit shown in Fig. 5 and the measured and fitted frequency responses of the filters near resonance are shown in Figs. 11 and 12. The values for the electrical components are listed in Table II for comparison. C_p is the static capacitance at each port to ground and is estimated using the layout of the electrodes and the thickness of the piezoelectric layer. C_m is calculated using the C_p value and the electromechanical coupling for the fourth-order thickness-extensional mode. L_m is then determined from the center frequency. Values of the feedthrough capacitance and the resistive elements are chosen to best fit the measured response. From Table II, it is seen that for the AlN filters, R_m as small as 4.5 Ω is achieved. The quality factor Q_m of the series resonance is 949, which is lower than that of commercial AlN-based FBARs. This provides a definite window of opportunity to improve the device performance. In comparison, the ZnO-on-Si filter has a significantly larger R_m of 14 Ω and smaller Q_m of 324. Small parallel resistances to C_p and C_f are needed for the ZnO-on-Si filter to account for the large loss tangent of ZnO.

The frequency response of the TPoS filters at different power levels is also tested. Fig. 13 shows the frequency response of the AlN-on-Si filter shown in Fig. 7 at input

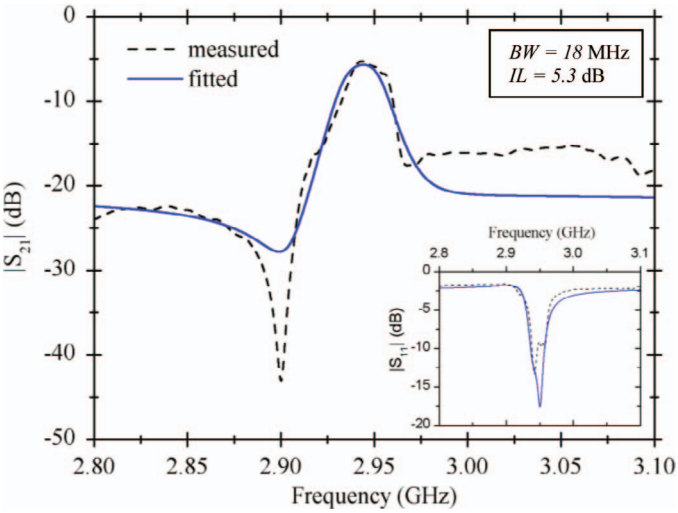

Fig. 11. Measured and fitted frequency responses of a ZnO-on-Si filter working at 2.94 GHz.

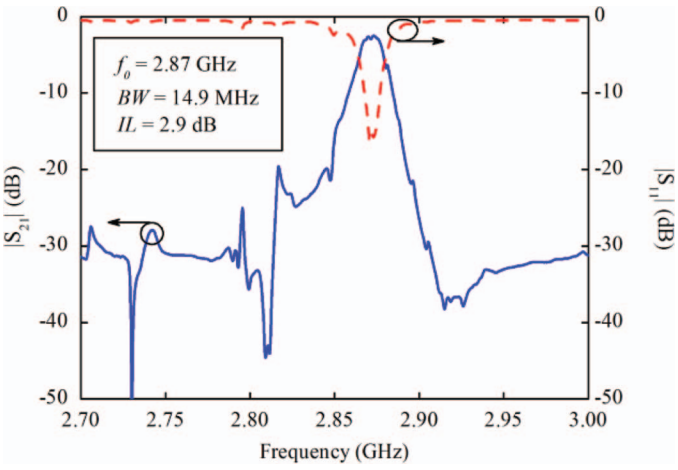

Fig. 10. Measured $|S_{21}|$ and $|S_{11}|$ of an AlN-on-Si filter (−5 dBm RF power). The filter consists of 20 pairs of 10-μm-wide electrode fingers separated by 5 μm gap.

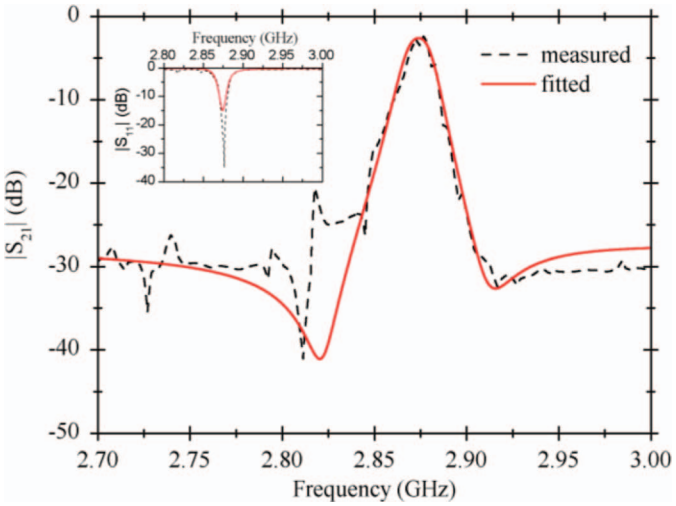

Fig. 12. Measured and fitted responses of an AlN-on-Si thin-film piezoelectric-on-substrate (TPoS) filter.

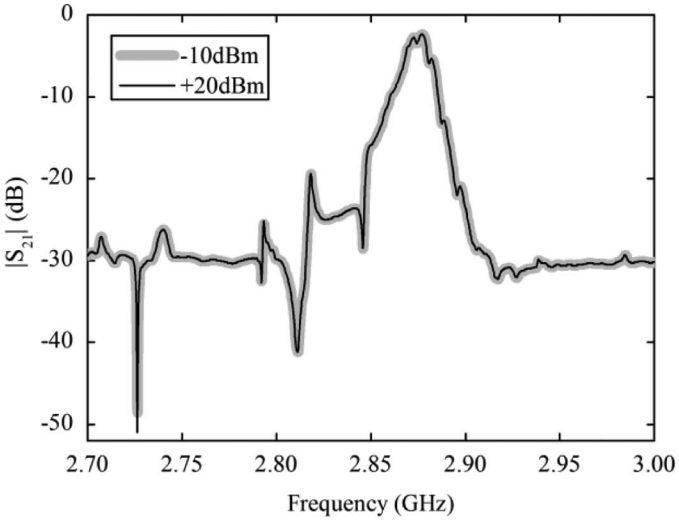

Fig. 13. The frequency response of the AlN-on-Si filter shown in Fig. 7 at different RF power levels.

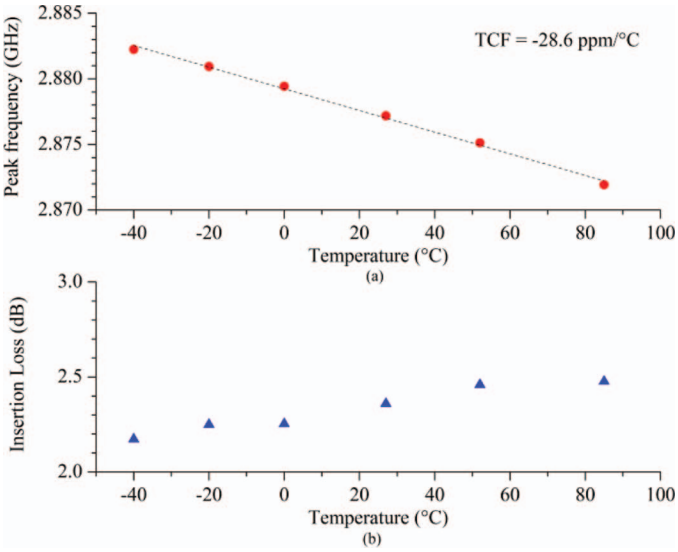

Fig. 14. (a) The peak frequency and (b) the insertion loss versus temperature plots of the thin-film piezoelectric-on-substrate (TPoS) filter shown in Fig. 7.

RF power levels of −10 dBm and +20 dBm. There is no visible change in the frequency response between the two power levels. To verify the power handling of the device, third-order intercept point (IIP_3) measurements are carried out using an N5214A Agilent PNA-X network analyzer in the two-tone source power mode. The measured IIP_3 of the device is better than +30 dBm, which is the measurement tool limit. Such power handling capability is attributed to the very good linearity of the Si substrate layer, as explained in detail in [23].

The temperature dependency of the filter is characterized by measuring the filter response using a Lakeshore cryogenic probe station (Lake Shore Cryotronics Inc., Westerville, OH). The measurement is carried out in a vacuum chamber from −40°C to +85°C with calibration done at each temperature point. The peak frequency versus temperature plot is shown in Fig. 14(a). The temperature coefficient of frequency (TCF) calculated from the linear fitting of the peak frequency and temperature is about −28.6 ppm/°C. Fig. 14(b) shows the dependency of insertion loss on temperature. From −40°C to +85°C, the insertion loss increases from 2.17 to 2.48 dB. The frequency shift induced by temperature change is comparable to the bandwidth of the filter. A temperature-stable design, either by intrinsic compensation or by tuning, may be desired in many applications. Such compensation can be realized by the introduction of a compensating layer, such as SiO_2, in the structure [24], or by the heavy doping of the silicon substrate [25] as demonstrated in other similar composite structures.

In a wider frequency spectrum, the TPoS filter shows multiple resonance peaks corresponding to various plate wave modes. In addition to the the pure thickness-extensional modes, other spurious modes may exist in the frequency range of interest, as can be seen in Fig. 15. To obtain a cleaner response, cascading of a TPoS filter with a wider-band preselect filter or an antenna may be necessary. One such example was presented in [26], in which an acoustic filter and a low-loss band-pass LC filter of 300 MHz bandwidth are cascaded to attenuate signal levels outside the passband.

VI. Conclusion

In this work, we presented the basic design and analysis of acoustically coupled AlN-on-Si thickness-mode filters. As a proof of concept, a band-pass filter was reported with an insertion loss of 2.4 dB and bandwidth of 12 MHz at 2.877 GHz. We compared the measured response with the dispersion curves and observed that the bandwidth of the fabricated filter is less than the trapping range for the stack. This indicates the possibility of designing a much wider bandwidth by optimizing the top electrode layout. The effect of top electrode layout on the filter frequency response is discussed in detail in Part II.

TABLE II. Equivalent Circuit Element Values for the AlN-on-Si and ZnO-on-Si Filters Shown in Figs. 11 and 12.

Parameter	AlN-on-Si	ZnO-on-Si	Parameter	AlN-on-Si	ZnO-on-Si
R_m (Ω)	4.5	14	L_m (nH)	237.2	246
R_f (Ω)	3000	500	L_c (nH)	1.3	1.8
C_m (fF)	13	11.94	C_p (pF)	1.2	1.1
C_f (fF)	50	70	R_p (Ω)	2075	250

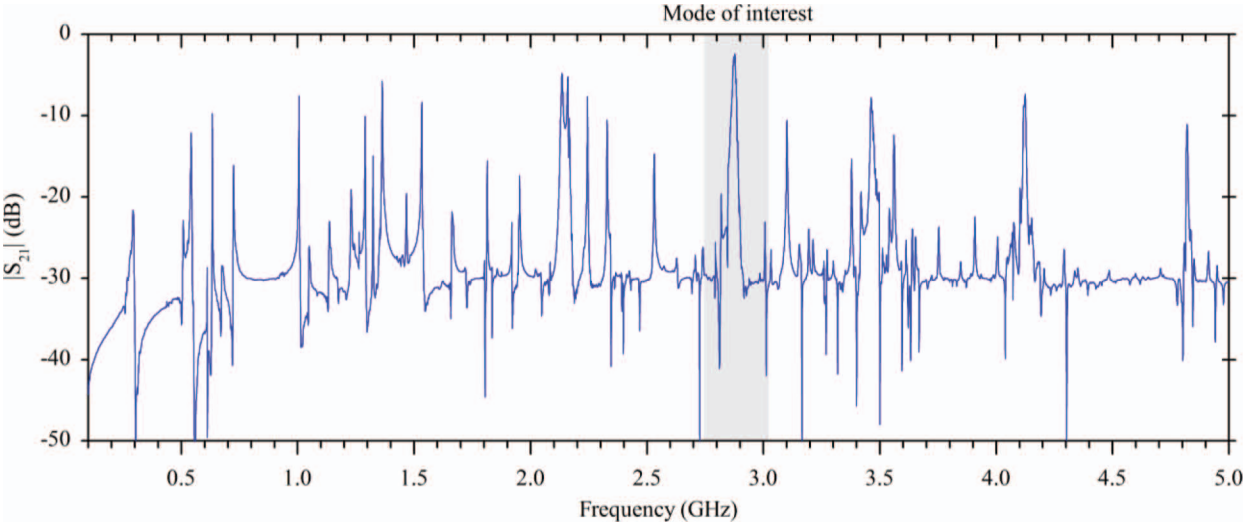

Fig. 15. The response of a thin-film piezoelectric-on-substrate (TPoS) filter measured in a wide frequency range.

Acoustically coupled TPoS filters feature a smaller chip size compared with ladder-type electrically coupled filters. These features, in addition to their excellent linearity at elevated RF power levels, make them ideal candidates for applications in commercial hand-held devices.

References

[1] P. Bradley, J. Kim, S. Ye, P. Nikkei, S. Bader, and C. Feng, "2X size and cost reduction of film bulk acoustic resonator (FBAR) chips with tungsten electrodes for PCS/GPS/800 MHz multiplexers," in *Proc. IEEE Ultrasonics Symp.*, 2007, pp. 1144–1147.

[2] R. F. Milsom, D. T. Elliott, S. Terry-Wood, and M. Redwood, "Analysis and design of coupled-mode miniature bar resonators and monolithic filters," *IEEE Trans. Sonics Ultrason.*, vol. 30, no. 3, pp. 140–155, May 1983.

[3] K. M. Lakin, "Coupled resonator filters," in *Proc. IEEE Ultrasonics Symp.*, 2002, pp. 901–908.

[4] R. Aigner, "SAW and BAW technologies for RF filter applications: A review of the relative strengths and weaknesses," in *Proc. IEEE Ultrasonics Symp.*, 2008, pp. 582–589.

[5] J. Kaitila, "Review of wave propagation in BAW thin film devices—Progress and prospects," in *Proc. IEEE Ultrasonics Symp.*, 2007, pp. 120 –129.

[6] W. Pan, R. Abdolvand, and F. Ayazi, "A low-loss 1.8 GHz monolithic thin-film piezoelectric-on-substrate filter," in *Tech. Dig. IEEE MEMS Conf.*, 2008, pp. 176–179.

[7] W. Pan and F. Ayazi, "Multiple-frequency thickness-mode thin-film piezoelectric-on-substrate filter array," in *Proc. IEEE Int. Frequency Control Symp.*, 2008, pp. 259–262.

[8] R. Abdolvand and F. Ayazi, "High-frequency monolithic thin-film piezoelectric-on-substrate filters," *Int. J. Microw. Wirel. Technol.*, vol. 1, no. 1, pp. 29–35, 2009.

[9] C. Ruppel and T. Fjeldly, *Advances in Surface Acoustic Wave Technology, Systems and Applications*, 1st ed., vol. 1, Singapore: World Scientific, 2001, pp. 72–75.

[10] V. A. Thakar, W. Pan, F. Ayazi, and M. Rais-Zadeh, "Acoustically coupled thickness-mode AlN-on-Si band-pass filters—Part II: Simulation and analysis," vol. 59, no. 10, pp. 2270–2277, 2012.

[11] *IEEE Standard on Piezoelectricity*, ANSI/IEEE Std. 176-1987, 1987, p. 59.

[12] W. Mason, "Equivalent electromechanical representation of trapped energy transducers," *Proc. IEEE*, vol. 57, no. 10, pp. 1723–1734, Oct. 1969.

[13] M. Lowe, "Matrix techniques for modeling ultrasonic waves in multilayered media," *IEEE Trans. Ultrason. Ferroelectr. Freq. Control*, vol. 42, no. 4, pp. 525–541, 1995.

[14] T. Pensala, J. Meltaus, K. Kokkonen, and M. Ylilammi, "2-D modeling of laterally acoustically coupled thin film bulk acoustic wave resonator filters," *IEEE Trans. Ultrason. Ferroelectr. Freq. Control*, vol. 57, no. 11, pp. 2537–2549, Nov. 2010.

[15] W. Beaver, "Theory and design principle of the monolithic crystal filter," Ph.D. dissertation, Dept. of Electrical Eng., Lehigh University, Bethlehem, PA, 1967.

[16] L. Dworsky, "An improved circuit model for monolithic crystal filters," *IEEE Trans. Sonics Ultrason.*, vol. 28, no. 4, pp. 283–284, Jul. 1981.

[17] R. Abdolvand, G. K. Ho, J. Butler, and F. Ayazi, "ZnO-on-nanocrystalline diamond lateral bulk acoustic resonators," in *Tech. Dig. IEEE MEMS Conf.*, 2007, pp. 795–798.

[18] A. Ansari, V. J. Gokhale, V. A. Thakar, J. Roberts, and M. Rais-Zadeh, "Gallium nitride-on-silicon micromechanical overtone resonators and filters," in *Proc. IEEE Electron Devices Meeting*, 2011, pp. 20.3.1–20.3.4.

[19] L. Lian and N. R. Sottos, "Effects of thickness on the piezoelectric and dielectric properties of lead zirconate titanate thin films," *J. Appl. Phys.*, vol. 87, no. 8, pp. 3941–3949, 2000.

[20] J. G. Gualtieri, J. A. Kosinski, and A. Ballato, "Piezoelectric materials for acoustic wave applications," *IEEE Trans. Ultrason. Ferroelectr. Freq. Control*, vol. 41, no. 1, pp. 53–59, 1994.

[21] T. E. Murphy, D. Y. Chen, and J. D. Phillips, "Growth and electronic properties of ZnO epilayers by plasma-assisted molecular beam epitaxy," *J. Electron. Mater.*, vol. 34, no. 6, pp. 699–703, 2005.

[22] K. M. Lakin, J. Belsick, J. F. McDonald, and K. T. McCarron, "Improved bulk wave resonator coupling coefficient for wide bandwidth filters," in *Proc. IEEE Ultrasonics Symp.*, 2001, vol. 1, pp. 827–831.

[23] R. Abdolvand and F. Ayazi, "Enhanced power handling and quality factor in thin-film piezoelectric-on-substrate resonators," in *Proc. IEEE Ultrasonics Symp.*, 2007, pp. 608–611.

[24] K. Nakamura, H. Sasaki, and H. Shimizu, "ZnO/SiO_2-diaphram composite resonator on a silicon wafer," *Electron. Lett.*, vol. 17, pp. 507–509, Jul. 1981.

[25] A. Samarao and F. Ayazi, "Temperature compensation of silicon micromechanical resonators via degenerate doping," in *IEEE Int. Electron Devices Meeting*, 2009, pp. 789–792.

[26] M. Rais-Zadeh, A. Kapoor, H. M. Lavasani, and F. Ayazi, "Fully integrated low-loss band-pass filters for wireless applications," *J. Micromech. Microeng.*, vol. 19, no. 8, pp. 525–542, Jul. 2009.

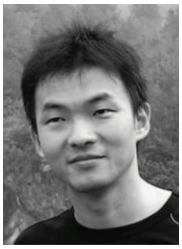

Wanling Pan (S'04–M'06) was born in 1980. He received his B.E. degree in electronic engineering from Tsinghua University, China, in 2000, and his Ph.D. degree in electrical engineering from the Katholieke Universiteit Leuven, Belgium, in 2006. From 2006 to 2009, he was a postdoctoral fellow in the School of Electrical and Computer Engineering, Georgia Institute of Technology, Atlanta, GA. He is currently with Integrated Device Technology Inc., San Jose, CA. His research interests include

the design, fabrication, and characterization of MEMS devices, with a focus on micro-resonators and filters.

Vikram Thakar (S'12) is a doctoral candidate in the Department of Mechanical Engineering at the University of Michigan. He received his B.E. degree in mechanical engineering from the University of Pune, India, in 2006 and his M.E. degree in integrated microsystems from the University of Michigan, Ann Arbor, in 2011. His research interests are in the areas of resonant micromechanical devices, acoustically coupled micromechanical resonators, and piezoelectrically actuated resonators for oscillator applications. The main focus of his research is on the relation between device modeling and fabrication as applied to the MEMS domain.

Mina Rais-Zadeh (S'03–M'08) received the B.S. degree in electrical engineering from the Sharif University of Technology, Tehran, Iran, and the M.S. and Ph.D. degrees in electrical and computer engineering from the Georgia Institute of Technology, Atlanta, GA, in 2005 and 2008, respectively. From August 2008 to 2009, she was a Postdoctoral Research Fellow with the Integrated MEMS Group, Georgia Institute of Technology. Since January 2009, she has been with the University of Michigan, Ann Arbor, where she is currently an Assistant Professor in the Department of Electrical Engineering and Computer Science. Her research interests include passive micromachined devices for communication applications, resonant micromechanical devices, gallium nitride MEMS, and micro/nano fabrication process development. Prof. Rais-Zadeh is the recipient of the NSF CAREER Award in 2011, the IEEE Electron Device Society Early Career Award in 2011, and finalist in the student paper competitions at the SiRF (2007) and IMS (2011) conferences. She serves as a member of the technical program committees of IEEE IEDM, IEEE Sensors, and the Hilton Head workshop.

Farrokh Ayazi (S'96–M'00–SM'05) is a Professor in the School of Electrical and Computer Engineering at the Georgia Institute of Technology and a director of the Center for MEMS and Microsystems Technologies (CMMT) at Georgia Tech. He received the B.S. degree in electrical engineering from the University of Tehran, Iran, in 1994 and the M.S. and Ph.D. degrees in electrical engineering from the University of Michigan, Ann Arbor, in 1997 and 2000, respectively. His research interests are in the areas of integrated micro and nano electromechanical resonators, inertial sensors, and interface IC design for MEMS and sensors. Dr. Ayazi is an editor for the *IEEE/ASME Journal of Microelectromechanical Systems*, and the *IEEE Transactions on Electron Devices*. He is a 2004 recipient of the NSF CAREER Award, the 2004 Richard M. Bass Outstanding Teacher Award (determined by the vote of the ECE senior class), and the Georgia Tech College of Engineering Cutting Edge Research Award for 2001–2002. He and his students won the best paper awards at Transducers 2011, the IEEE International Frequency Control Symposium in 2010, and IEEE Sensors conference in 2007.

Dr. Ayazi is the Co-Founder and Chief Technology Officer of Qualtré Inc., a spin-out from his research laboratory that commercializes multi-axis bulk acoustic wave silicon gyroscopes and six-degrees-of-freedom inertial sensors for consumer electronics and personal navigation systems.